

# Normal and inverse spin-valve effect in organic semiconductor nanowires and the background monotonic magnetoresistance

Sandipan Pramanik and Supriyo Bandyopadhyay\*

*Department of Electrical and Computer Engineering, Virginia Commonwealth University, Richmond, Virginia 23284, USA*

Kalyan Garre and Marc Cahay

*Department of Electrical and Computer Engineering and Computer Science, University of Cincinnati, Cincinnati, Ohio 45221, USA*

(Received 12 September 2006; published 29 December 2006)

We have observed both peaks and troughs in the magnetoresistance of organic nanowires consisting of three layers—cobalt, 8-hydroxy-quinolinolato aluminum (Alq<sub>3</sub>), and nickel. They always occur between the coercive fields of the ferromagnetic layers, and we attribute them to the normal and inverse spin-valve effect. The latter is caused by resonant tunneling through localized impurity states in the organic material. Peaks are always found to be accompanied by a positive monotonic background magnetoresistance, while troughs are accompanied by a negative monotonic background magnetoresistance. This curious correlation suggests that the background magnetoresistance, whose origin has hitherto remained unexplained, is probably caused by the recently proposed phenomenon of magnetic-field-induced enhancement of spin-flip scattering in the presence of spin-orbit interaction [Cahay and Bandyopadhyay, *Phys. Rev. B* **69**, 045303 (2004)].

DOI: [10.1103/PhysRevB.74.235329](https://doi.org/10.1103/PhysRevB.74.235329)

PACS number(s): 72.25.Rb, 72.25.Mk, 72.25.Hg, 72.25.Dc

## I. INTRODUCTION

There is significant interest in studying spin-polarized transport in organic semiconductors because of its possible applications in organic spintronics.<sup>1-13</sup> One of the most widely studied organic systems in this context is the *spin valve* consisting of an organic layer sandwiched between two ferromagnetic electrodes. These structures (and/or their derivatives) typically show a large background monotonic magnetoresistance in addition to the (nonmonotonic) spin-valve resistance peak occurring between the coercive fields of the two ferromagnetic contacts. The background magnetoresistance can be either positive or negative. Its origin has remained a mystery. Organic layers that do not have ferromagnetic contacts also show a monotonic magnetoresistance and some attempts have been made to explain that by invoking weak localization and antilocalization.<sup>3</sup> These are rather unlikely causes since the magnetoresistance is typically observed up to room temperature.<sup>3</sup> Localization or antilocalization requires preservation of quantum mechanical phase coherence of charge carriers over long distances. That is unlikely to happen at room temperature, particularly in organics where transport occurs mainly via phonon-assisted hopping. In this paper, we focus on the background magnetoresistance observed in spin-valve structures with ferromagnetic contacts. An exhaustive study of nanowire organic spin-valve structures has been carried out and we have found an intriguing correlation between the sign of the spin-valve peak and the sign of the background magnetoresistance. Based on that, we offer an explanation for the background magnetoresistance in spin-valve structures, which does not require phase coherence and therefore can explain its occurrence at relatively high temperatures. We emphasize that our explanation depends on spin-polarized transport and therefore cannot explain the magnetoresistance observed in Refs. 2 and 3 which used nonmagnetic contacts for carrier injection and extraction.

This paper is organized as follows. We first describe the spin-valve device and the significance of the spin-valve peak in the magnetoresistance, as well as what might determine its sign. In Sec. III, we describe fabrication of the nanowire organic spin valves. Results are presented in Sec. IV and discussion in Sec. V, and we conclude in Sec. VI.

## II. THE SPIN-VALVE DEVICE

A spin valve is a trilayered structure, in which a paramagnetic spacer layer is sandwiched between two ferromagnetic electrodes of different coercivities. The resistance of this device depends on the relative magnetization orientations of the ferromagnetic contacts. The spin-valve signal is the ratio

$$\frac{\Delta R}{R} = \frac{R_{AP} - R_P}{R_P} \quad (1)$$

where  $R_{AP}$  and  $R_P$  denote the device resistance when the magnetizations of the two ferromagnetic contacts are antiparallel and parallel, respectively. If the spin polarizations at the Fermi energy in both ferromagnets have the same sign, meaning that the majority spins in one ferromagnet are also majority spins in the other (an example being the case of cobalt and nickel), then  $R_{AP} > R_P$  and the above ratio should be positive.

Consider now a spin-valve device—with cobalt and nickel contacts—placed in a magnetic field. At high magnetic fields, both ferromagnets are magnetized along the direction of the field and hence their magnetizations are parallel. Accordingly, the device resistance is low. As the field is decreased, swept past zero, and then reversed, the ferromagnet with the lower coercivity (nickel) reverses its magnetization, thus placing the two ferromagnets in the antiparallel configuration. The device resistance now increases. As the field strength is further increased in the reverse direction, the second ferromagnet (cobalt) also reverses its magnetization

as its coercive field is exceeded. Thereupon, the two magnetizations again become parallel and the device resistance falls. This causes a nonmonotonic peak in the magnetoresistance occurring between the coercive fields of the two ferromagnets. This is the spin-valve peak and its height above the background resistance is the quantity  $\Delta R$ . It is positive if  $R_{AP} > R_P$ . The positive peak is a manifestation of the *normal* spin-valve effect.

It is possible to extract the spin diffusion length in the spacer layer from the height of the spin-valve peak. If the spacer is a semiconductor material, there exists a Schottky barrier at the ferromagnet/semiconductor interface. Under the influence of an applied bias, carriers are injected from the ferromagnet into the semiconductor via tunneling through this barrier with a surviving spin polarization  $P_1$ . As long as the barrier is thin enough, we can ignore any loss of spin polarization in traversing the barrier and assume that  $P_1$  is approximately the spin polarization of the density of states at the Fermi energy in the injecting ferromagnet. After injection, carriers drift and diffuse through the spacer with exponentially decaying spin polarization given by  $P_1 \exp[-x/\lambda]$  where  $x$  is the distance traveled and  $\lambda$  is the spin diffusion length in the spacer. Finally the carriers transmit through the tunnel (Schottky) barrier at the interface of the spacer and the second ferromagnet. If we apply the Julliere formula<sup>14</sup> at this “detecting” interface, then we get

$$\frac{\Delta R}{R} = \frac{2P_1P_2e^{-L/\lambda}}{1 - P_1P_2e^{-L/\lambda}} \quad (2)$$

where  $P_2$  is the spin polarization of the density of states at the Fermi energy of the second (i.e., detecting) ferromagnet and  $L$  is the length of the spacer layer. This model has been used in Ref. 13 to determine the spin relaxation length  $\lambda$  in organics from the measured spin-valve signal  $\Delta R/R$ . This model ignores any possible loss of spin polarization at the interfaces between the organic and either ferromagnetic contact. Organics have a so-called “self-adjusting” capability which was invoked in Ref. 13 to justify this model.

If there are localized defects in the organic material and carriers resonantly tunnel through them, then the spin polarization of the ferromagnetic contact nearer to the defect can be effectively inverted (sign reversed).<sup>15,16</sup> In that case,  $P_1$  and  $P_2$  will have opposite signs, implying  $R_{AP} < R_P$ . This will produce a *negative* spin-valve signal and a negative spin-valve peak  $\Delta R$ . In other words, the peak becomes a trough. This is the *inverse* spin-valve effect.

We have observed both peaks and troughs in nanowires of 8-hydroxy-quinolinolato aluminum ( $\text{Alq}_3$ ) sandwiched between cobalt and nickel electrodes, i.e., we have observed the normal spin-valve effect in some samples and the inverse spin-valve effect in others. The organic material is a small-molecular-weight compound semiconductor. This material is commonly used as the electron transport and light emission layer in organic light-emitting diodes.

In addition to the spin-valve peak or trough, we always observe a ubiquitous background monotonic magnetoresistance defined as  $\delta R(|B|) = R(|B|) - R(0)$ , where  $B$  is the magnetic flux density. Whenever the spin-valve signal is nega-

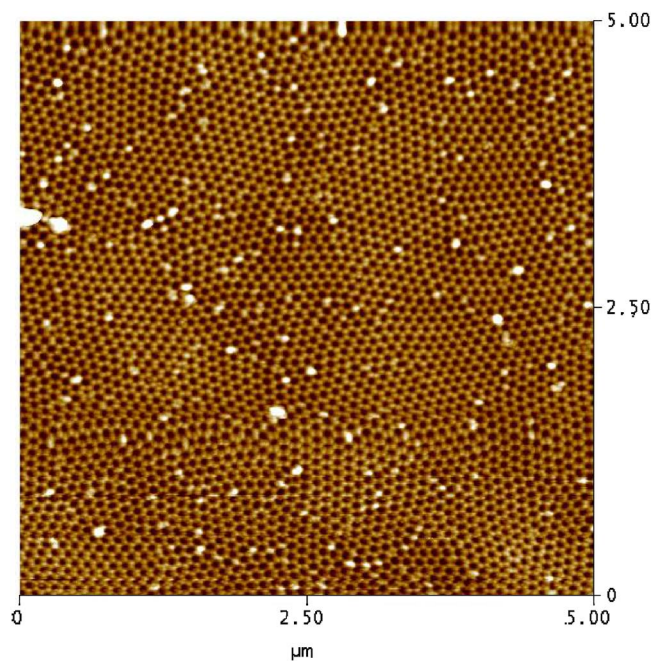


FIG. 1. (Color online) Atomic force microscopy (AFM) image of the top surface of the alumina template formed by anodization using 3% oxalic acid at 40 V dc. Pore diameter  $\sim 50$  nm.

tive, the sign of the magnetoresistance  $\delta R(|B|)$  is also negative, and when the spin-valve signal is positive, the sign of  $\delta R(|B|)$  is positive. This curious correlation sheds light on the likely origin of the magnetoresistance.

### III. FABRICATION OF NANOWIRE ORGANIC SPIN VALVES

The nanowire spin-valve structures are self-assembled using an electrochemical technique. We electropolished<sup>17</sup> and then anodized a high-purity metallic aluminum foil (0.1 mm thick) in 0.3M oxalic acid with an anodization voltage of 40 V dc. This produces a porous alumina film on the surface of the foil with nominal pore diameter of 50 nm (Fig. 1) and areal pore density of  $2 \times 10^{10} \text{ cm}^{-2}$ .<sup>18</sup> The anodization is carried out for 10 min to produce a  $\sim 1\text{-}\mu\text{m}$ -thick alumina film and therefore yield pores that are  $\sim 1 \mu\text{m}$  deep. At the bottom of the pores, there is a  $\sim 20\text{-nm}$ -thick layer of alumina known as the “barrier layer.” This layer is removed by a reverse polarity etching procedure<sup>19</sup> so that the underlying aluminum is exposed at the bottom of the pores. To confirm that the barrier layer has been indeed removed, we have stripped off the aluminum substrate in some samples by soaking in  $\text{HgCl}_2$  solution to release the porous alumina film and obtained atomic force micrographs from the back side of the film as shown in Fig. 2. Pores are visible on the back side of the film, indicating that we have obtained “through-hole” nanopores on the surface of bulk aluminum. This through-hole structure allows dc electrodeposition of materials selectively inside the pores, since it makes the conducting aluminum substrate electrically accessible at the pore bottom. At the same time, this allows us to perform transport measure-

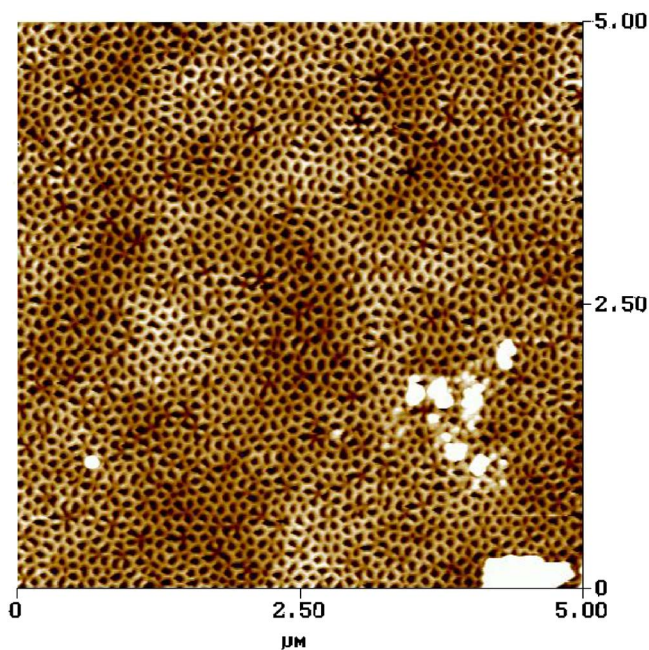


FIG. 2. (Color online) AFM image of the bottom surface of the alumina template after removing bulk alumina. We observe “through pores” as a result of reverse polarity etching.

ments on the electrodeposited nanowires (passing current along the length of the nanowires). Note that almost all pores are open at the bottom so that the vast majority of the nanowires will be electrically contacted from the bottom.

Next, we electrodeposit nickel within the pores from a (mildly acidic) solution of  $\text{NiSO}_4 \cdot 6\text{H}_2\text{O}$  by applying a dc bias of 1.5 V at a platinum counterelectrode with respect to the aluminum substrate. A small deposition current ( $\sim$ microamperes) ensures well-controlled and slow-but-uniform electrodeposition of Ni inside the pores. We calibrated the deposition rate of Ni under these conditions by monitoring the deposition current during electrodeposition of Ni inside pores of known length. The deposition current increases drastically when the pores are completely filled and a nickel percolation layer begins to form on the surface. The deposition rate is determined by calculating the ratio of pore length to pore filling time. According to this calibration, the thickness of the nickel layer (deposited inside the pore) is approximately 500 nm. Transmission electron microscopy (TEM) characterization of these Ni nanowires showed that the wire lengths are almost uniform and indeed conform to  $\sim$ 500 nm. These samples are air dried and then  $\text{Alq}_3$  is thermally evaporated on top of the Ni layer through a mask with a window of area  $1 \text{ mm}^2$  in a vacuum of  $10^{-6}$  Torr, the rate of deposition being in the range 0.1–0.5 nm/s. During evaporation,  $\text{Alq}_3$  seeps into the pores by surface diffusion and capillary action, and reaches the nickel. The fact that  $\text{Alq}_3$  is a short-stranded organic of low molecular weight is helpful in transporting it inside the pores. The thickness of the evaporated  $\text{Alq}_3$  layer is monitored by a crystal oscillator and subsequently confirmed by TEM analysis. In this study the thickness of the  $\text{Alq}_3$  layer is  $\sim$ 25 nm (see Fig. 3). Finally, cobalt is evaporated on the top without breaking vacuum. The resulting structure is schematically depicted in

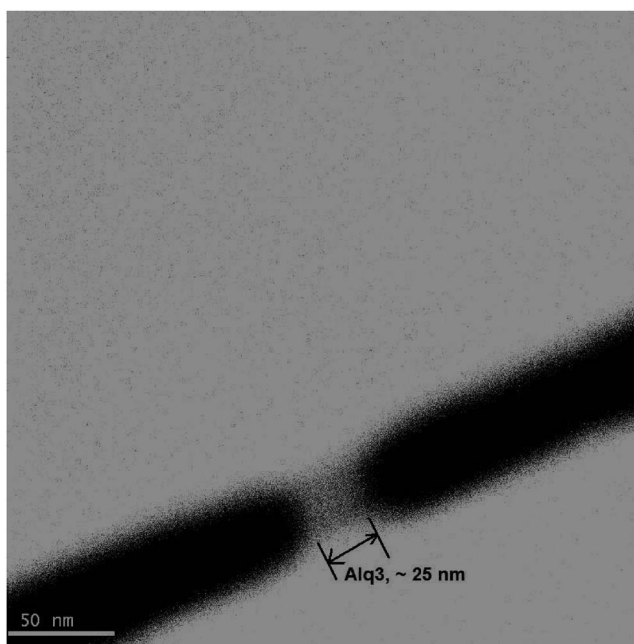


FIG. 3. Transmission electron micrograph of a single nanowire showing the  $\text{Alq}_3$  layer sandwiched between the cobalt and nickel electrodes. This image was produced by releasing the nanowires from the alumina host by dissolution of alumina in dilute phosphoric acid and capturing the nanowires on TEM grids for imaging.

Fig. 4. The thickness of the cobalt layer (as deposited inside the pores) is also  $\sim$ 500 nm since the total pore length is  $\sim$ 1  $\mu\text{m}$ . Thus, we end up with an array of *nominally identical* spin-valve nanowires. Since the cobalt contact pad has an area of  $\sim$ 1  $\text{mm}^2$ , approximately  $2 \times 10^8$  nanowires are electrically contacted in parallel (the areal density of the nanowires is  $2 \times 10^{10} \text{ cm}^{-2}$ ). Note that the surrounding alumina

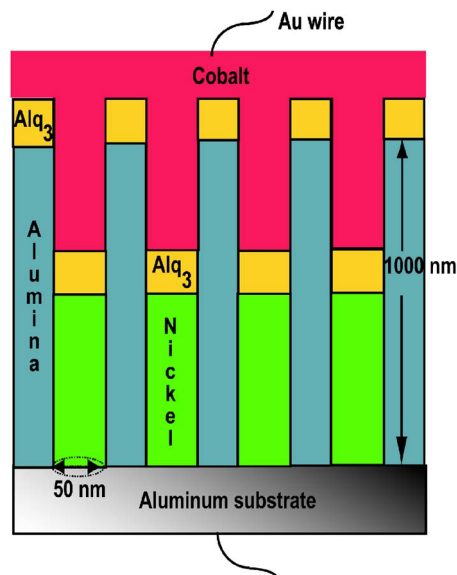


FIG. 4. (Color online) Schematic representation of the nanowire organic spin-valve device. The nanowires are hosted in an insulating porous alumina matrix and are electrically accessed from each end. The magnetic field is applied along the axis of the wire.

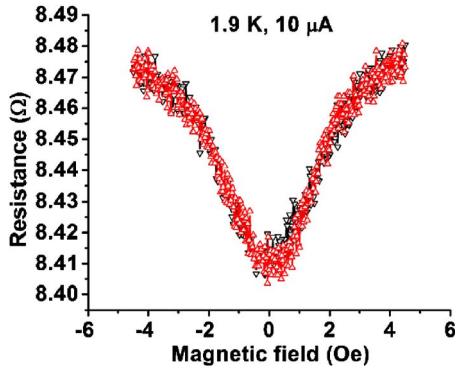


FIG. 5. (Color online) Magnetoresistance trace of the control sample, consisting of  $\sim 500$  Ni-Co bilayered nanowires (no Alq<sub>3</sub>).

walls provide a natural encapsulation and protect the Alq<sub>3</sub> layer from moisture contamination. For electrical measurements, gold wires are attached to the top cobalt layer and the bottom aluminum foil with silver paste.

#### IV. RESULTS

From measured conductivity values, we can estimate the number of nanowires that are electrically connected from both ends. For example, the resistivity of an Alq<sub>3</sub> thin film is typically  $10^5 \Omega \text{ cm}$  at room temperature.<sup>20</sup> When Alq<sub>3</sub> is confined in pores, we assume that the resistivity increases by an order of magnitude because of the increase in surface scattering. This is a typical assumption used in similar contexts.<sup>21</sup> Therefore, the resistivity of Alq<sub>3</sub> nanowires is  $10^6 \Omega \text{ cm}$ . The resistivities of the ferromagnetic nanowire electrodes are  $\sim 10^{-3} \Omega \text{ cm}$ .<sup>21</sup> Thus the resistance of a single trilayered nanowire is  $10^{11} \Omega$ . Since the resistance of the sample is  $\sim 1 \text{ k}\Omega$ , we estimate that 50% of the nanowires ( $\sim 10^8$ ) under the cobalt layer are electrically connected from both ends. Note that, since the resistivity of Alq<sub>3</sub> is nine orders of magnitude larger than the resistivities of the ferro-

magnets, during transport experiments, we will always probe the resistance of the Alq<sub>3</sub> layer only, and not the resistance of the ferromagnetic electrodes, which are in series with the Alq<sub>3</sub> layer. Thus, all features in the resistance accrue from the organic layer and have nothing to do with the ferromagnetic contacts. Consequently, if there are features originating from the anisotropic magnetoresistance effects in the ferromagnets, we will never see them.

To confirm that the contribution of the ferromagnetic layers to the resistance of the structure is indeed negligible, we fabricated a set of control samples without any Alq<sub>3</sub> layer. Note that a parallel array of  $2 \times 10^8$  Ni/Co bilayered nanowires (contacted by Al at the bottom and a thin film of Co at the top with area  $1 \text{ mm}^2$ ) would produce a resistance of  $\sim 25 \mu\Omega$ , which is below the sensitivity of our measurement apparatus. Therefore, we made control samples where we probe only  $\sim 500$  nanowires. The trick employed to achieve this was to remove the barrier layer incompletely from the bottom (intentionally), so that only a small fraction of the pores opened up from the bottom. We measure a resistance of  $\sim 10 \Omega$  in the control samples at room temperature, which tells us that about 500 nanowires are electrically probed.

The magnetoresistances of the control samples were measured in a Quantum Design Physical Property Measurement System with an ac bias current of  $10 \mu\text{A}$  rms, over a magnetic field range of 0–6 kOe and at a temperature of 1.9 K. This system has a superconducting coil within a cryostat that generates a magnetic field along the axis of the nanowires. A typical trace is shown in Fig. 5. We never observed any magnetoresistance peak or trough in these samples, but observed a monotonic positive magnetoresistance  $\delta R(|B|)$  which accrues either from the anisotropic magnetoresistance effect associated with the ferromagnetic contacts or from the magnetoresistance of the aluminum substrate. However, the maximum value of  $\delta R(|B|)$  that we observed over the entire measurement range was only  $\sim 0.08 \Omega$ , which is more than an order of magnitude smaller than the resistance peak  $\Delta R$  measured in the trilayered structures (see later). Thus, the resistance peak measured in the trilayered structures un-

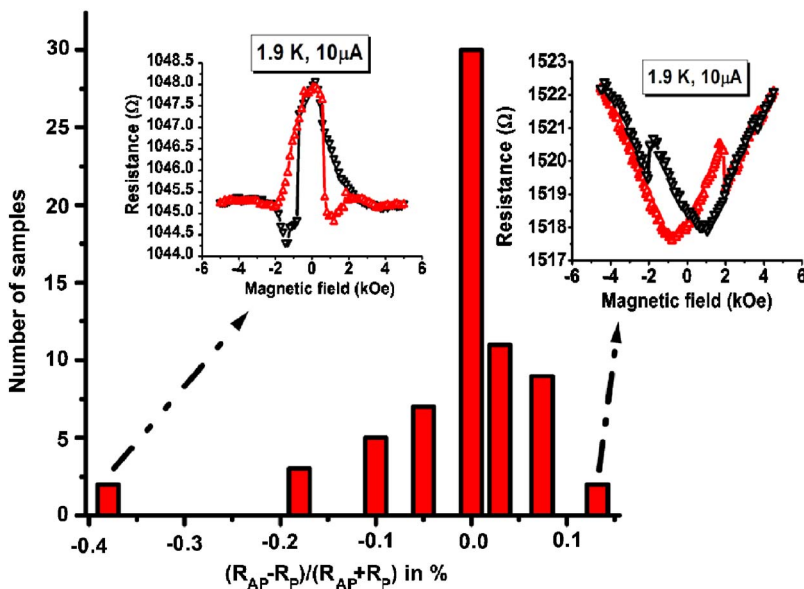


FIG. 6. (Color online) Histogram showing the distribution of spin-valve signal strength collected over 90 samples. Some of these samples show a positive spin-valve signal and the rest a negative spin-valve signal. All of these data were collected at a bias current of  $10 \mu\text{A}$ .

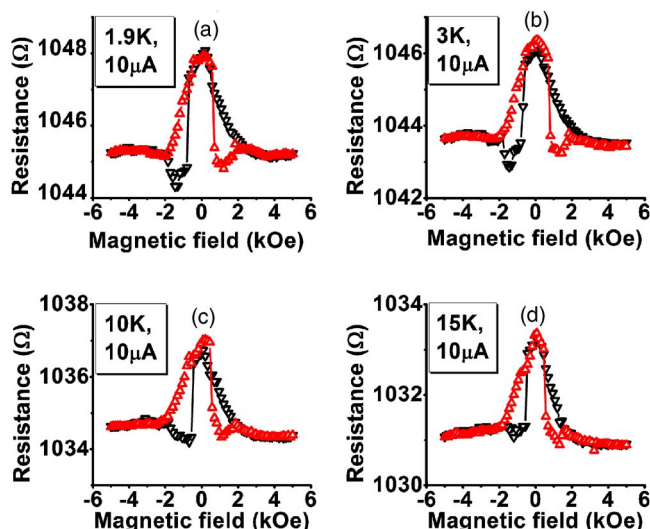


FIG. 7. (Color online) Inverse spin-valve effect and background negative magnetoresistance in Ni-Alq<sub>3</sub>-Co nanowires at four different temperatures and fixed bias (10  $\mu$ A).

doubtedly originates from the spin-valve effect and has nothing to do with either the anisotropic magnetoresistance associated with the ferromagnetic contacts, or the magnetoresistance of the aluminum substrate.

We fabricated  $\sim 90$  trilayered samples using the procedure described in Sec. III. Room-temperature resistances of these samples range from 1 to 10 k $\Omega$  depending on the number of nanowires that are electrically contacted from both ends (this number varies because the process of barrier layer removal is not precisely controllable). The magnetoresistance of these samples was measured in a Quantum Design Physical Property Measurement System with an ac bias current of 10  $\mu$ A rms over a temperature range 1.9–100 K and over a magnetic field range of 0–6 kOe. The measured distribution of spin-valve signal  $\Delta R/R$  is shown in Fig. 6. The distribution is very broad and peaks near zero, i.e., most samples do not exhibit any measurable spin-valve signal. Among the remaining samples, some exhibit positive spin-valve signals (peaks) and others exhibit negative signals (troughs).

The insets of Fig. 6 show the magnetoresistance traces for the highest positive and negative spin-valve signals that we have measured among all samples tested. In every sample, the spin-valve peak always occurs between the coercive fields of Ni ( $\sim 800$  Oe) and Co ( $\sim 1800$  Oe) nanowires, as expected. Surprisingly, we found that the coercive fields do not vary significantly from sample to sample, indicating that the variation of coercive fields between different nanowires, and therefore different samples, is extremely small. The magnetoresistances of the devices exhibiting the inverse spin-valve effect typically saturate at low fields (0.2 T in the figure shown), but those of devices exhibiting the normal spin-valve effect tend to saturate at much higher fields.

Figure 7 shows the magnetoresistance traces of a sample exhibiting a negative spin-valve signal at four different temperatures. The bias current is kept constant at 10  $\mu$ A rms. The spin-valve signal decreases with increasing temperature, indicating that the spin diffusion length in the organic mate-

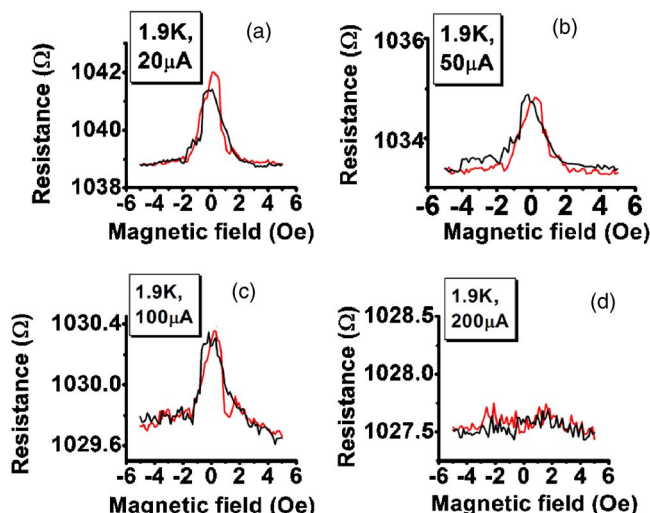


FIG. 8. (Color online) Inverse spin-valve effect and background negative magnetoresistance in Ni-Alq<sub>3</sub>-Co nanowires at four different bias values and fixed temperature (1.9 K).

rial decreases with increasing temperature. The temperature dependence of the spin diffusion length and spin relaxation time in these samples, over a temperature range 1.9–100 K, was presented in Ref. 10. Based on the temperature dependence and other features, we concluded in Ref. 10 that the main spin relaxation mechanism in the nanowires is the Elliott-Yafet mode associated with elastic collisions.

Figure 8 shows the bias current dependence of the negative spin-valve signal in a typical sample at a constant temperature of 1.9 K. As the bias current is increased, the spin-valve signal decays rapidly and at 200  $\mu$ A, no signal is measurable with our apparatus. This happens because with increased bias current, there is increased carrier scattering which leads to more rapid spin relaxation and a shorter spin diffusion length. The spin-valve signal has an inverse exponential dependence on the ratio of the device length to the spin diffusion length. As the latter decreases, the spin-valve signal becomes increasingly weaker, and ultimately imperceptible. The high current, however, does not destroy the sample irreversibly. As the current is decreased, the spin-valve signal is recovered.

Figure 7 also shows that there is a background monotonic magnetoresistance  $\delta R(|B|)$  accompanying the spin-valve signal and its sign is negative [ $R(|B|) < R(0)$ ]. We found consistently that, whenever the spin-valve signal is negative, the background magnetoresistance is also negative, and whenever the spin-valve signal is positive, the background magnetoresistance is positive (see the insets of Fig. 6). The background magnetoresistance has very little sensitivity to temperature (Fig. 7), but it is extremely sensitive to bias, as can be seen in Fig. 8. It disappears at a bias current of 200  $\mu$ A.

## V. DISCUSSION

The origins of the positive (normal) and negative (inverted) spin-valve peak were discussed in Sec. II. The nega-

tive (inverted) spin-valve peak (or trough) is manifested when carriers resonantly tunnel through a localized defect or impurity state in the organic material. This requires that the carrier energy is resonant with the impurity level. In some nanowires, this may happen, and they exhibit a trough. In others, this does not happen so that they exhibit a peak, instead of a trough. Since each sample consists of a large number ( $\sim 10^8$ ) of nanowires, there is some cancellation between the positive and negative signals, which decreases the measured signal as a result of ensemble averaging. This is probably the reason why the distribution in Fig. 6 peaks near zero.

We will now explain why a peak is accompanied by a positive background magnetoresistance and a trough is accompanied by a negative background magnetoresistance. At any magnetic field, except between the coercive fields of the two ferromagnets, the magnetizations of the injecting and detecting contacts are parallel. Assume also that both ferromagnets have the same sign of the spin polarization (as is indeed the case with cobalt and nickel). Now consider the case when the spin-valve peak is positive, meaning that there is no resonant tunneling through impurity states, resulting in an effective inversion of the spin polarization of the nearest contact. In this case, an injected carrier will transmit and contribute to current if its spin does not flip within the spacer layer. In the presence of spin-orbit interaction, a magnetic field will increase the spin-flip rate by inducing spin mixing.<sup>22,23</sup> Thus, the probability of spin flipping increases with increasing magnetic field. If the injected carrier's spin flips, then it will be blocked by the detecting contact and the current will decrease, resulting in an increase in resistance. Thus, the resistance should increase with increasing magnetic field, resulting in a *positive* background monotonic resistance. This is what we observe.

In the case of negative spin-valve signal, resonant tunneling through an impurity state results in effective inversion of the spin polarization of the nearer ferromagnetic contact. In this case, spin flipping within the spacer layer will allow the flipped spin to transmit through the detector contact, which would have otherwise blocked it. Thus spin-flip events decrease the device resistance, instead of increasing it. Since a magnetic field increases the spin-flip rate, the resistance will decrease with increasing magnetic field, resulting in a negative monotonic background resistance. Again, this is exactly what we observe.

These mechanisms are illustrated in Fig. 9.

Note that the above mechanism for the background monotonic magnetoresistance does not call for phase coherence of charge carriers and therefore can persist up to high temperatures. Of course, this mechanism is spin dependent and therefore does not explain the magnetoresistance observed in Ref. 3 which used nonmagnetic contacts. This mechanism requires correlation of the signs of the spin-valve signal and the background magnetoresistance. If they turn out to be anticorrelated, then this will not be the cause. We have always observed correlation, and never observed anticorrelation, in all our experiments (90 samples, multiple traces). Therefore, we believe the mechanism suggested here is indeed the likely cause.

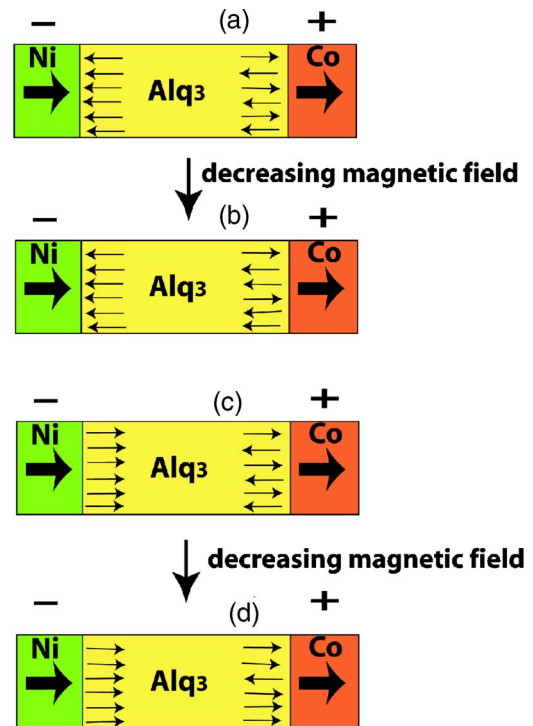


FIG. 9. (Color online) Explanation of the relation between the sign of the background magnetoresistance and the sign of the spin-valve peak. (a) Consider the case when  $H > |H_{Co}| > |H_{Ni}|$  and inversion of injected spin polarization has taken place due to resonant tunneling through an impurity somewhere in the channel. We assume that the impurity is closer to the Ni contact so that the spin polarization of the Ni contact has been effectively reversed as shown in the figure. Owing to the high magnetic field, the spin relaxation rate is high (Ref. 23) and the injected spins are completely depolarized by the time they reach the Co/Alq<sub>3</sub> interface. Therefore, on the average, 50% of the spins have their polarizations aligned along the magnetization of the Co contact and are transmitted by the Co contact. The device resistance =  $R_1$  (say). (b) When the magnetic field is decreased so that  $H = 0+$ , the spin relaxation rate falls. Only partial depolarization of the spins occurs as the carriers traverse the channel, so that fewer than 50% of the spins have their polarizations aligned along the magnetization of the Co contact and are transmitted. In this case, the device resistance is  $R_2$  which is larger than  $R_1$ . This explains why the background magnetoresistance is negative whenever there is resonant inversion and a resulting negative spin-valve peak. (c) Again, consider the case when  $H > |H_{Co}| > |H_{Ni}|$  but no resonant inversion of injected spin polarization takes place. The high magnetic field completely depolarizes the injected spins by the time they reach the Co contact (owing to the high spin-flip rate) and again 50% of the carriers are transmitted. The device resistance is  $R'_1$ . (d) When the field is reduced to  $H = 0+$ , only partial depolarization takes place and more than 50% of the spins are aligned along the Co contact's magnetization. Therefore more than 50% of the spins are transmitted and the device resistance is smaller than  $R'_1$ . This explains why the background magnetoresistance is positive whenever there is no resonant inversion so that the spin valve peak is positive. Note that this physics is somewhat counterintuitive. At high magnetic fields, one would expect that the spins would remain aligned along the field and more of them will transmit through the Co contact. Just the opposite happens because the magnetic field increases the spin-flip rate and contributes to depolarization.

## VI. CONCLUSION

In conclusion, we have studied spin transport in organic nanowire spin valves and found an intriguing correlation between the sign of the spin-valve signal and the background monotonic magnetoresistance. Based on this correlation, we have proposed a likely origin of the background magnetoresistance.

## ACKNOWLEDGMENT

This work was supported by the National Science Foundation under Grant No. ECS-0608854. This work was also supported by the US Air Force Office of Scientific Research under grant FA9550-04-1-0261.

\*Corresponding author. Email address: sbandy@vcu.edu

- <sup>1</sup>V. Dediu, M. Murgia, F. C. Maticotta, C. Taliani, and S. Barbarera, *Solid State Commun.* **122**, 181 (2002).
- <sup>2</sup>O. Mermer, G. Veeraraghavan, T. L. Francis, and M. Wohlgenannt, cond-mat/0501124 (unpublished).
- <sup>3</sup>O. Mermer, M. Wohlgenannt, G. Veeraraghavan, D. Wu, and T. L. Francis, cond-mat/0312204 (unpublished).
- <sup>4</sup>T. L. Francis, O. Mermer, G. Veeraraghavan, and M. Wohlgenannt, *New J. Phys.* **6**, 185 (2004).
- <sup>5</sup>A. H. Davis and K. Bussmann, *J. Appl. Phys.* **93**, 7358 (2003).
- <sup>6</sup>E. Arisi, I. Bergenti, V. Dediu, M. A. Loi, M. Muccini, M. Murgia, G. Ruani, C. Taliani, and R. Zamboni, *J. Appl. Phys.* **93**, 7682 (2003).
- <sup>7</sup>E. Shikoh, Y. Ando, and T. Miyazaki, *J. Magn. Magn. Mater.* **272**, 1921 (2004).
- <sup>8</sup>Y. Yoshida, A. Fujii, M. Ozaki, K. Yoshino, and E. L. Frankevich, *Mol. Cryst. Liq. Cryst.* **426**, 19 (2005).
- <sup>9</sup>M. Wohlgenannt, Z. V. Vardeny, J. Shi, T. L. Francis, X. M. Jiang, O. Mermer, G. Veeraraghavan, and Z. H. Xiong, *IEE Proc.: Circuits Devices Syst.* **152**, 385 (2005).
- <sup>10</sup>S. Pramanik, C.-G. Stefanita, S. Bandyopadhyay, N. Harth, K. Garre, and M. Cahay, cond-mat/0508744 (unpublished).
- <sup>11</sup>P. P. Ruden and D. L. Smith, *J. Appl. Phys.* **95**, 4898 (2004).
- <sup>12</sup>Z. G. Yu, M. A. Berding, and S. Krishnamurthy, *IEE Proc.: Circuits Devices Syst.* **152**, 334 (2005).
- <sup>13</sup>Z. H. Xiong, D. Wu, Z. V. Vardeny, and J. Shi, *Nature (London)*

**427**, 821 (2004).

- <sup>14</sup>M. Julliere, *Phys. Lett.* **54A**, 225 (1975).
- <sup>15</sup>E. Y. Tsymbal, O. N. Mryasov, and P. R. LeClair, *J. Phys.: Condens. Matter* **15**, R109 (2003).
- <sup>16</sup>E. Y. Tsymbal, A. Sokolov, I. F. Sabirianov, and B. Doudin, *Phys. Rev. Lett.* **90**, 186602 (2003).
- <sup>17</sup>S. Bandyopadhyay, A. E. Miller, H. C. Chang, G. Banerjee, V. Yuzhakov, D.-F. Yue, R. E. Ricker, S. Jones, J. A. Eastman, E. Baugher, and M. Chandrashekar, *Nanotechnology* **7**, 360 (1996).
- <sup>18</sup>H. Masuda and M. Satoh, *Jpn. J. Appl. Phys., Part 2* **35**, L126 (1996).
- <sup>19</sup>O. Rabin, P. R. Herz, S. B. Cronin, Y. M. Lin, A. I. Akinwande, and M. S. Dresselhaus, in *MRS Symposia Proceedings No. D.4.7.1*, edited by J. A. Rogers, A. Karim, L. Merhari, D. Norris, and Y. Xia (Materials Research Society, Pittsburgh, 2001), p. 636.
- <sup>20</sup>A. K. Mahapatro, R. Agrawal, and S. Ghosh, *J. Appl. Phys.* **96**, 3583 (2004).
- <sup>21</sup>S. Pramanik, C. G. Stefanita, and S. Bandyopadhyay, *J. Nanosci. Nanotechnol.* **6**, 1973 (2006).
- <sup>22</sup>M. Cahay and S. Bandyopadhyay, *Phys. Rev. B* **68**, 115316 (2003).
- <sup>23</sup>M. Cahay and S. Bandyopadhyay, *Phys. Rev. B* **69**, 045303 (2004).